

Quality Metrics and Reliability Analysis of Laser Communication System

A. Arockia Bazil Raj* and S. Padmavathi#

**Electronics Engineering, Defence Institute of Advanced Technology, Pune, India*

#*Computer Science & Engineering, Thiagarajar College of Engineering, Madurai, India*

**E-mail: brazilraj.a@gmail.com*

ABSTRACT

Beam wandering is the main cause for major power loss in laser communication. To analyse this prerequisite at our environment, a 155 Mbps data transmission experimental setup is built with necessary optoelectronic components for the link range of 0.5 km at an altitude of 15.25 m. A neuro-controller is developed inside the FPGA and used to stabilise the received beam at the centre of detector plane. The Q-factor and bit error rate variation profiles are calculated using the signal statistics obtained from the eye-diagram. The performance improvements on the laser communication system due to the incorporation of beam wandering mitigation control are investigated and discussed in terms of various communication quality assessment key parameters.

Keywords: Laser communication, weather data, beam wandering; neuro-controller, Q-factor, atmospheric attenuation, bit error rate

1. INTRODUCTION

The features of Laser communication technology make it more viable when compared with other existing radio frequency (RF), microwave and millimeter wave based wireless communication and networking technologies¹⁻⁴. This is due to various key advantages which include un-regulated (free of government regulation) and license free transmission bandwidth spectrum, a large data transmission (at the order of multiple gigabits per second), consumption of low power, security (cannot penetrate walls), low installation and operational cost, quick deployment (smaller size and weight), last-mile access, fiber backup, back-haul for wireless cellular networks, high-definition television transmission as well as freedom from electro-magnetic interference and electro-magnetic compatibility^{1,3,5,6}. As an alternative to RF technology, the laser communication system appears very appealing in meeting the future demand for broadband internet access, ubiquitous and broadcasting services^{7,8}. Laser communication does not incur high cost in digging of tunnels and trenching of roads to install bulky copper and fiber cables^{5,8}. Therefore, the installation and maintenance cost of a laser communication link is much lower than the RF and fiber based links^{8,9}. Laser communication is also believed to play an important role in the future satellite networks and space scientific exploration that include:

- (i) satellite cross links,
- (ii) satellite to aircraft,
- (iii) aircraft to aircraft, and
- (iv) ground station to aircraft and/or satellite and vice-versa^{6,8,10,11}.

Portability of the laser communication is leading for the establishment of temporary links for high speed information flows in big cities and industrial complexes^{8,10,11}.

In metropolitan area network, laser communication can be used to enable LAN connectivity and intercampus links, since, laser communication is an excellent candidate for last-mile connectivity^{2,5,11}. To support high bandwidth services, the use of microwave or millimeter wave systems will be required. But, in these systems, device technology is currently either expensive or immature^{1,6,8,11}. Further, the RF spectrum is already exceedingly congested and frequency allocations of sufficient bandwidths are extremely hard to obtain^{1,6,11}.

Despite these advantages, the performance of the laser communication link largely depends on the weather conditions since its channel is atmospheric turbulent medium as in Fig. 1 and its successful deployment is limited by several key problems associated with the weather data^{5,6,10}. This is primarily because of factors such as the unpredictability of the FSO channel effects at the optical frequencies as well as difficulties associated with stabilising the transmitting and receiving platforms against wind and other disturbing agents which affect the quality of beam alignment, power fluctuations (intensity noise) and wavefront aberration (phase noise)^{8,12-14}. Optical beam propagation through the turbulent atmospheric channel severely suffers from the atmospheric attenuation (A_{att}), angular deflection and phase distortion in horizontal (terrestrial) propagation rather than the vertical^{6,8,14,15}. Attenuation here is described as photons being extinguished. In the case of a laser beam, attenuation rather leads to a displacement of the excitation than to photons being extinguished. In addition, atmospheric turbulence also leads to phase-front distortions resulting, for example, in deflection of the beam i.e., beam wander¹²⁻¹⁵. All these effects result in both average received power loss and instantaneously received power fluctuation, called fading, at the receiver aperture. This leads to increased

system bit error rate (BER), decreased channel capacity and reliability of the overall system^{6,10,11,16}. These effects interrupt the high data rate of laser communication link from achieving the availability of five nines^{6,8,10} i.e., 99.999 per cent. One approach to address these problems is increasing the optical power level launched into the air when the propagation loss becomes high. However, the use of high-power optical fiber amplifiers (OFAs) as boosters will increase the cost steeply^{6,8}.

Another approach for reducing the optical power fading is using slightly diverged beam and receiving it via larger size aperture telescope^{4,6,8}. However, a diverged beam usually causes significant loss of average received power and large aperture telescope generally collects more background optical noise as well. Therefore, the benefits of increasing the optical power and/or using slightly diverging beam with larger receiver aperture (larger than or close to the long term laser spot size) may not balance the laser communication performance loss/degradation¹⁴⁻¹⁶. Therefore, laser communication is still considered as an emerging technology and is widely being researched, particularly with regard to the mitigation/compensation of signal degradation caused by the turbulent atmosphere^{6,14,15}. These are all the general problems that require attention to be dealt with. The major impact on the laser communication data link due to the random fluctuations of the atmospheric turbulence is as follows:

- (i) optical scattering and observation (characterised by A_{att}),
- (ii) random optical power fluctuation (characterised by scintillation index),
- (iii) beam wandering i.e., beam surface global (temporal) tilt due to beam centroid displacement on the detector plane (characterised by effective scintillation index) and
- (iv) wavefront distortions i.e., beam surface (spatial) local tip-tilt (characterised by the Zernike polynomials)^{3,13,14,17}.

The conventional data coding and/or modulation techniques can effectively be used to equalise/compromise the first two effects with respect to the weather condition at a given instant of time. The third and fourth effects can't be resolved without incorporating the adaptive optics i.e., beam stabilisation and wavefront aberration correction elements^{4,12-}

¹⁶. Resolving these problems is mandatory for the successful installation of the laser communication system^{8,9,14,15}. One of the main reasons for the failure of laser communication is the absence of beam pointing, acquisition and tracking (PAT) system and therefore, a perfect and continuous adaptive alignment is important to reduce the pointing loss^{3,4,14,15}. To demonstrate this, a mandatory requirement for the successful installation of the laser communication system, a real-world open atmospheric optical data transmission system, as in Fig. 1, with necessary optoelectronic assembly as shown in Fig. 2. Transmitter (T_x) and receiver (R_x), is established and used to conduct the terrestrial (on-ground) experimental study to characterize the laser communication system behaviour with and without mitigating the beam wandering effects. The Q-factor, atmospheric transmittance (T_a), BER, beam centroid stabilisation, A_{att} , voltage distribution of the received signal and atmospheric turbulence strength (C_n^2) are continuously measured, recorded and on/off line analysis are carried out in MATLAB environment in order to intensively investigate the performance improvement in the received beam centroid stability at the detector plane due to incorporating the beam wandering mitigation (BWM) control.

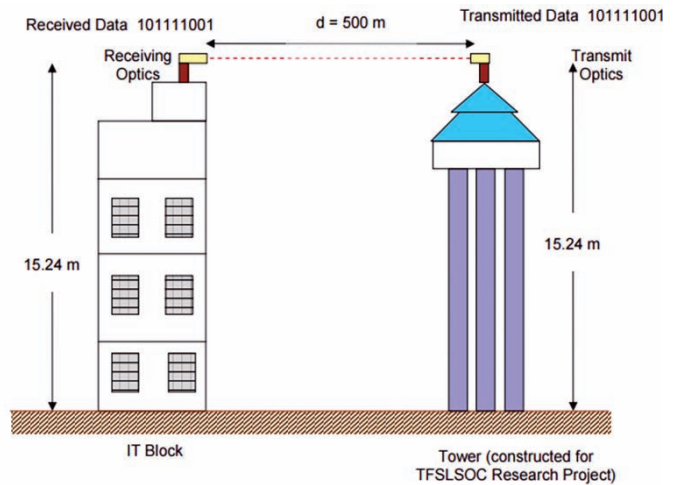


Figure 1. Overall layout of laser communication link.

RECEIVER (R_x)

TRANSMITTER (T_x)

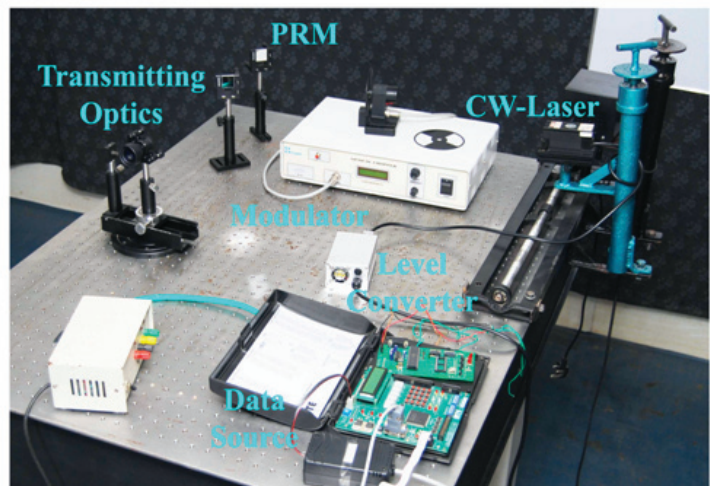
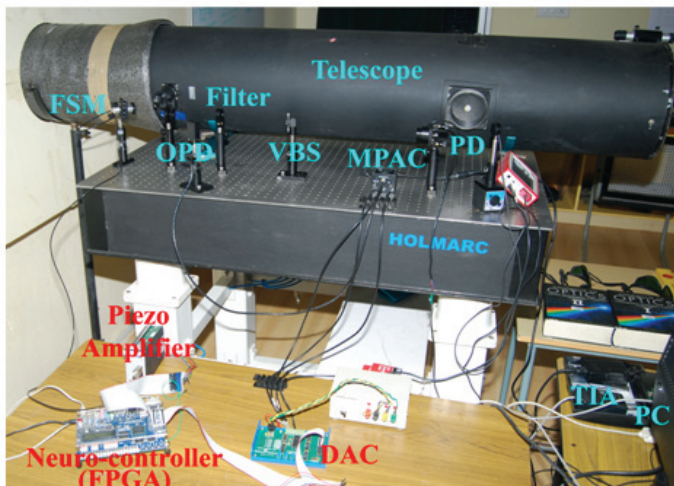


Figure 2. Snapshot showing the opto-electronic components assembly at the transmitter and receiver laboratories.

2. QUANTITATIVE EVALUATION OF CHANNEL EFFECTS AND BER

In the communication point of view, there are many factors that become critical when evaluating the performance of the laser communication system which relies on a travelling wave generated by a laser source at certain transmitted power (P_t) and wavelength (λ). The average optical power available at the receiver (P_r) at a distance of 'R' km is approximated by⁶

$$P_r = P_t \frac{D_r^2}{D_t^2 + (R\theta)^2} \exp\left(-\frac{\theta_{pe}^2}{(\theta/2)^2}\right) T_a T_r \quad (1)$$

where D_t and D_r are diameter of the transmitting optics and receiving telescope aperture respectively, θ is laser beam full-angle divergence, θ_{pe} is pointing error and T_r is transmittance of the receiving optics. During data transmission, the angle between the T_x and R_x line of sight and the transmitting beam axis must be kept within a fraction of the transmitting beamwidth which may be as smaller as a few micro-radians as discussed in Section-I. In laser communication, the fluctuations of the P_r have to be related with the A_{att} and C_n^2 to characterise the turbulent channel effects on the propagated data carrying optical beam^{8,10,18-23}. The data carrying modulated optical beam cannot be used to measure the A_{att} and the C_n^2 since it bears data (information) and its average power get fluctuated at the receiver plane due to the modulation of the beam even under a favorable atmospheric condition^{21,23}. One way of simultaneously measuring the A_{att} and C_n^2 is using a separate unmodulated optical setups/link, i.e., beacon beam, parallel to the data bearing optical path as a transmissometer for A_{att} and scintillometer for C_n^2 as detailed^{6,18,21,23}. This approach will increase the overall cost of the system. Furthermore, the atmospheric effect mitigation system is required to stabilize this beam also. Therefore, models yielding more accurate estimation of A_{att} (dB/km) and C_n^2 ($m^{-2/3}$) according to the local weather data at our test field are formulated as described^{21,23}, and given in Eqns. (2) and (3). The estimated C_n^2 is categorised as very-weak ($C_n^2 < 10^{-16}$), weak ($10^{-16} m^{-2/3} \leq C_n^2 < 10^{-15} m^{-2/3}$), moderate ($10^{-15} m^{-2/3} \leq C_n^2 < 10^{-14} m^{-2/3}$), strong ($10^{-14} m^{-2/3} \leq C_n^2 < 10^{-13} m^{-2/3}$), and very-strong⁸ ($C_n^2 \geq 10^{-13} m^{-2/3}$).

$$A_{att} = C_0 + C_1 Ws + C_2 T + C_3 RH + C_4 Ws^2 + C_5 WsT + C_6 WsRH + C_7 T^2 + C_8 TRH + C_9 RH^2 + C_{10} Ws^3 + C_{11} T^3 + C_{12} RH^3 \quad (2)$$

where $C_0 = -1.09$, $C_1 = -3.18$, $C_2 = 2.49$, $C_3 = 0.27$, $C_4 = 0.06$, $C_5 = 0.03$, $C_6 = 0.02$, $C_7 = -0.10$, $C_8 = 0.006$, $C_9 = -0.01$, $C_{10} = -0.006$, $C_{11} = 0.001$, and $C_{12} = 9.56 e^{-5}$. The T_a is calculated in per cent by substituting the values of A_{att} estimated using Eqn. (2) in the Beer Lambert law as detailed in^{6,8,23} and the maximum transmittance (T_{amax}) is obtained when the A_{att} is minimum.

$$C_n^2 = 1 \times 10^{-14} (C_0 + C_1 Ws + C_2 + C_3 RH + C_4 Ws^2 + C_5 WsT + C_6 WsRH + C_7 TRH + C_8 Ws^3 + C_9 T^3 + C_{10} TRH^2 + C_{11} RH^3 + C_{12} Ws^4 + C_{13} Ws^3 T + C_{14} Ws^3 RH + C_{15} Ws^2 T^2 + C_{16} Ws^2 RH^2 + C_{17} T^4 + C_{18} T^3 RH + C_{19} T^2 RH^2 + C_{20} RH^3 Ws + C_{21} RH^3 T + C_{22} RH^4) \quad (3)$$

where $C_0 = 5360.63$, $C_1 = 21.04$, $C_2 = -281.76$, $C_3 = -63.55$, $C_4 = -0.04$, $C_5 = -0.10$, $C_6 = -0.27$, $C_7 = 2.19$, $C_8 = -0.26$, $C_9 = 0.19$, $C_{10} = 0.01$, $C_{11} = 5.79 e^{-4}$, $C_{12} = -1.44 e^{-3}$, $C_{13} = 0.01$, $C_{14} = 9.24 e^{-4}$, $C_{15} = -1.59 e^{-3}$, $C_{16} = 1.18 e^{-4}$, $C_{17} = -2.65 e^{-3}$, $C_{18} = -4.36 e^{-4}$, $C_{19} = -3.33 e^{-4}$, $C_{20} = 7.60 e^{-6}$, $C_{21} = -6.82 e^{-5}$, and $C_{22} = 1.65 e^{-6}$. In this work, the Q-factor is obtained using the constructed eye-diagram and BER is measured using Keysight N4902B serial BER tester. The maximum Q-factor i.e., Q_{max} is computed as a function of T_{amax} and received signal statistics by^{3,6,8}

$$Q_{max} = T_{amax} \left(\frac{I_1 - I_0}{\sigma_0 + \sigma_1} \right) \quad (4)$$

where I_1, I_0 are average detected signal current for bit '1' and '0' respectively, σ_0, σ_1 are variance of received bits '0' and '1' respectively and determined using the constructed eye-diagram. The attenuated Q-factor (Q_{Att}) is estimated in terms of the maximum Q-factor and the T_a during different C_n^2 conditions by^{3,8}

$$Q_{Att} = T_a Q_{max} \quad (5)$$

The BER for the NRZ-OOK modulation format is calculated by^{3,6,8}

$$BER = \frac{1}{2} \operatorname{erfc} \left(\frac{Q_{Att}}{\sqrt{2}} \right) \quad (6)$$

The Eqns. (4) - (6) are used to measure/analyse the received data quality on the basis of estimated signal and noise statistics. Moreover, the magnitude considered to estimate the laser communication system in this work is the average capacity that indicates the average best data rate for error-free transmission i.e., average BER and outage probability.

3. EXPERIMENTAL SETUP AND DESIGN OF NEURAL-CONTROLLER

This section speaks the description of the experimental opto-electronics assembly and functionality of the neuro-controller.

3.1 Description on the Experimental Setup

A simplex laser communication data link experimental setup as shown in Figs. (1) and (2) is built for a link range of 0.5 km at an altitude of 15.25 m. The experimental test-beds consist of data source, level converter, optical modulator, Laser source, pure reflection mirror and transmitting optics

at the transmitter and telescope, fast steering mirror (FSM), narrow band interference optical filter (NBIOF), variable beam splitter (VBS), opto-electronic position detector (OPD), mono-pulse arithmetic circuit (MPAC), data acquisition card (DAC), neuro-controller, piezo-amplifier, photodiode, trans impedance amplifier (TIA), real time scope, optical power meter and data logging computer at the receiver. All these opto-electronics components are mounted on the vibration damped optical bread boards as shown in Fig. 2. The schematic diagram of the experimental setup is shown in Fig. 3. A Pseudo random binary sequence (PRBS) serial data generator's output²⁴ is given as the input to optical modulator, through an unipolar to bipolar level convertor, to modulate the 850 nm, 10 mW optical beam at the asynchronous transfer mode (ATM) rate of 155 Mbps. A widely using OOK modulation scheme is used to directly modulate the optical signal^{6,8,10,15}. Transmitting optics is used to increase the beam diameter from 3 mm to 9 mm, such as to significantly reduce the beam divergence at the aperture of the receiver^{18,21}.

Intensity modulated optical beam is made to propagate through real-world open atmosphere and to be available at the aperture of the receiver. Telescope captures all optical power and reflects to fall on the FSM. The FSM consists of three terminal piezoelectric actuators based moving platform on which the beam steering mirror is mounted^{3,8,14,21}. The incident laser beam of FSM gets reflected to the beam splitter, through NBIOF, which splits the incident beam into reflecting and propagating beams. The reflected beam is made to fall on the photodiode followed by TIA and used for communication key parameters assessment. Equivalent photocurrent at the output of the photodiode (PD) is amplified using TIA. Output of the TIA is captured using a high-frequency real time oscilloscope in which full signal analysis are carried out during different C_n^2 conditions. The propagating beam (passed through the beam splitter) is made to fall on the OPD. The OPD and MPAC are the key devices involving for the measurements of beam wandering i.e., beam centroid position information^{3,9,16}. The OPD consists of four separate identical silicon photodiodes arranged in quadrant geometry¹⁶. These photodiodes convert

incident light into relative currents and then to relative voltage V_A, V_B, V_C , and V_D using the I-V converter. Voltage generated by each quadrant is proportional to optical energy illuminating its surface as presented in¹⁶. The outputs of the OPD are connected to the MPAC where the beam spot centroid displacement errors (normalised) σ_{Ex} and σ_{Ey} along the x and y-channel (2D Plane) are measured as the relative output voltage changes by^{3,8,16}

$$\sigma_{Ex} = \frac{(V_A + V_C) - (V_B + V_D)}{V_A + V_B + V_C + V_D}$$

$$\sigma_{Ey} = \frac{(V_A + V_B) - (V_C + V_D)}{V_A + V_B + V_C + V_D}$$
(7)

The MPAC output signals $\{\sigma_{Ex}, \sigma_{Ey}\}$ are applied to a 12-bit parallel data-fetching A/D (AD1674 converter core) through an eight-channel analog multiplexer (ADG509A) circuit. The digitised outputs are given to the neuro-controller built inside the FPGA via a very high density cable interconnect. The controller output data are converted to analog signal using D/A (DAC 7728 core) converter and given to the FSM through the piezo-amplifier in a closed-loop control configuration as in Fig. 3. The neuro-controller output signals drive the FSM in the counter (opposite) positions i.e., accomplishing the beam tilt in conjugate direction such as to mitigate the beam wander. The displacement error data, control signal and received data are continuously measured and simultaneously logged in the data logging computer (PC) through the UART-RS232 communication port.

3.2 Design and Functionality of the Neuro-controller

Beam position error inputs $\{E_x$ and $E_y\}$ and the corresponding control outputs $\{C_x, C_y\}$ are experimentally measured during the pilot survey using the developed experimental setup in open-loop control configuration as shown in Fig. 4. Although there are many parameters that affect the beam steering process in beam stabilisation, azimuth and elevation displacement errors contribute the greatest effect on the success of its operation^{9,15,16}. These parameters are

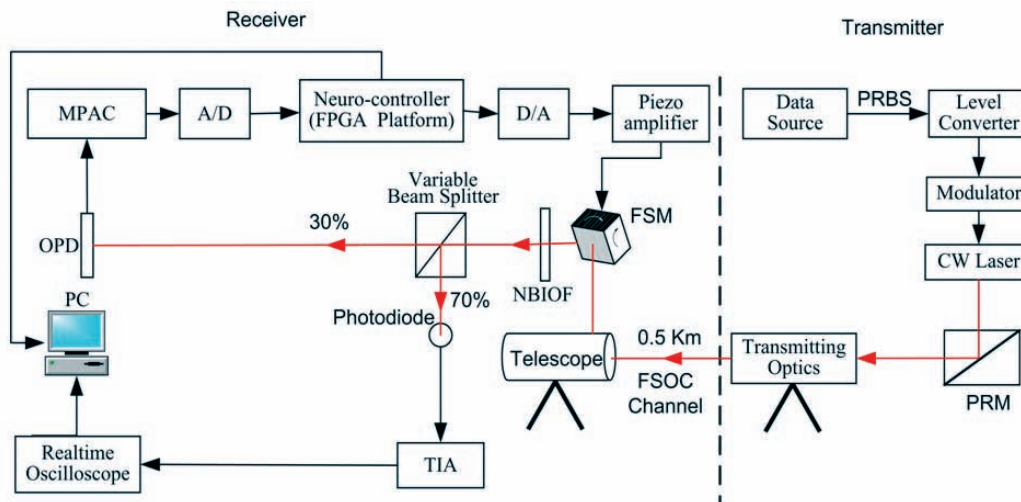


Figure 3. Schematic diagram of the laser communication experimental setup.

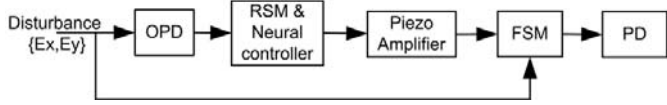


Figure 4. Neuro-controller in open-loop control for pilot survey experiment.

considered as the principal components in this work since they moreover directly affect beam stability and link quality. The neuro-controller is designed in order to accomplish the direct non-linear input-output mapping through which the beam wandering is mitigated^{3,9,16}. The pilot survey experimental results are used as the training data set to design an appropriate neural network pattern in the MATLAB environment. The mean square error of 10^{-6} is used as stopping criteria for the training process¹⁶. A 2-12-9-2 (2 neurons in the input layer (IL), 12 neurons in first hidden layer (HL1), 9 neurons in second hidden layer (HL2) and 2 neurons in the output layer (OL)) is the structure of the developed neuro-controller¹⁶. A coded pattern of the designed neural network is shown in Fig. 5.

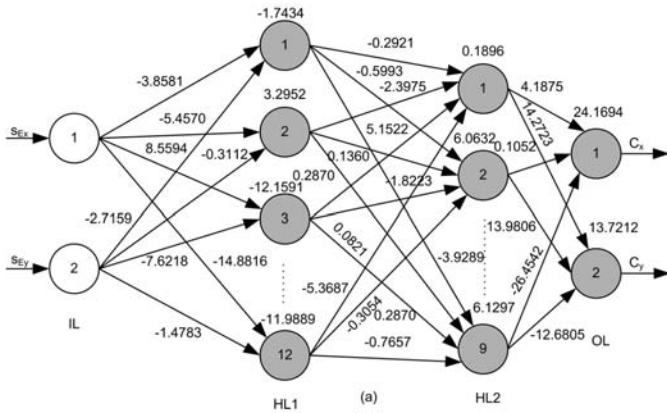


Figure 5. A pattern of trained neural network with weight and bias values.

The FPGA is popularly being used due to the advantages of low power, compactness, huge amount of pipelined parallel data processing and high speed computations especially for the neuro-controller implementation^{3,9}. Therefore, the neuro-controller is designed in MATLAB environment and implemented in FPGA. The mixed design environment: very high speed integrated circuit hardware description language and system generator tools, are used together due to the possibility of modeling and simulating the digital system from a high level of abstraction module designs⁹. A novel pipelined parallel architecture is developed inside the FPGA to implement the neuro-controller and deployed at the receiver experimental setup as shown in Fig. 3. The hardware design consists of six main modules namely (a) clock manager, (b) data pre-processor, (c) memory manager, (d) neuron unit, (e) data router, and (f) MAC unit. The signal transition flow through the main modules of the neuro-controller and their functionalities are as follows

(a) Clock Manager

The on-board clock frequency in the FPGA development board is 50 MHz. To achieve the required frequencies, the new

clock signals (sub clocks) have been synthesised by means of a digital clock manager provided in the FPGA^{3,9}. The clock manager outputs are given to the (i) internal shift controller, (ii) internal process controller, and (iii) enable signal generator at the specified synchronised frequencies for globally controlled data/command flow and operations.

(b) Data Pre-processor

This unit consists of two circuits, namely A/D interfacing architecture and pre-processor³. The data required to enable the analog multiplexer and channel select addresses are stored in the channel control register. The 12-bit output of A/D corresponding to the selected channel is forced to available at the input of the demultiplexer by asserting the output-enable control signal. The selective lines of the multiplexer and demultiplexer are synchronised with a finite-state machine for the proper data acquisition⁹. Once the content of all the registers are loaded, then the values are forwarded into the pre-processor module which performs the normalisation operation as described in²⁵ and the values are forwarded to the HL1 neuron for the rising edge of a clock signal and this state is maintained till accomplishing inputs and synaptic weight multiplications followed by the addition of bias for the HL1 computations.

(c) Memory Manager

The synaptic weights and bias values are stored in the on-board SDRAM. The organisation of weight and bias memory addresses are allocated based on the priority of data sequence forwarding for successive computations. The SDRAM units are constructed as a circular data shift register, so that it forwards the chosen weight and bias values to the feed-back path as well as to the multiplier in the feed-forward path as described in²⁵. Three 12-element row vectors, nine 12-element row vectors with one 9-element column vector and two 9-element row vectors with one 2-element column vector are the structure of the HL1, HL2 and OL memory, respectively³. The memory manager supplies the weight (w_1, w_2, w_3) and bias (b_1, b_2, b_3) values to the appropriate units whenever requested. The input, synaptic weight and bias value shifting are synchronised with the clock manager units and controlled by the weight and bias control signals.

(d) Neuron Unit

The neuron unit (activation function) is implemented to calculate the activation level (a) of net input (n) as $a = f(n)$; where f is the neuron function^{3,9}. The neurons in the HL1 and HL2 are bipolar sigmoidal activation functions and in the OL are bipolar linear activation functions. The bipolar sigmoidal activation function is implemented as a second-order non-linear function in FPGA as described²⁵. Only one neuron instead of 12 neurons in the HL1, 9 neurons in the HL2 and 2 neurons in the OL are implemented.

(e) Data Router

Two data routers are designed and used in such a way to utilise the minimum amount of hardware resources to feed the data to the multiply-accumulation (MAC) unit as a serial-in serial-out circular shift register for the HL2 and

OL configurations. The router units are developed based on the methodology of neuron configuration, i.e., one neuron or multiple neurons²⁵. A 1×12 demultiplexer is used in the first router and its first nine outputs are given in parallel to the HL2 MAC computations once in every 12 subsequent clocks. The outputs of the HL2 neurons are directly given to the OL router once in every 9 subsequent clock inputs^{3,9} and then repeated with a new set of input data. The first two register outputs are given in parallel to the OL MAC computations.

(f) MAC Unit

The single-precision (32-bit) floating point arithmetic standard is used for accomplishing the input and synaptic weight multiplications with bias additions²⁵. The nine MAC units for HL2 and two MAC units for OL are developed for neuron input computations. Once, a MAC operation for one complete set of inputs at first router is accomplished, the final result is forwarded to the bias addition in parallel for the rising edge of the command signal, so that, the final outputs, i.e., the inputs to the HL2 neurons are generated. Similarly, the second MAC unit section multiplies the outputs of the second router with the corresponding weights, accumulates the results and finally forwards to the bias addition in parallel, so that the OL neural inputs are generated.

As in Fig. 3, the beam position information is continuously being monitored/scanned by the neuro-controller at a sampling rate of 4 kHz. As soon as the beam position error is identified, the neuro-controller generates the control signal such as to steer the FSM to take the beam back to center of the OPD. That means, the error computation and control action are in a closed-loop control configuration. Therefore, the controller does not allow the beam to recede the center of the OPD. Once this stabilisation is accomplished, then the maximum energy will be coupled with the communication photodiode as in Figs. 3 and 4. The fundamental mathematical equations related to the neural network training, design algorithm, feed-forward multilayer perceptron design, digital architecture, open-loop and closed-loop control performance can be found in our previous works published in ^{3,9,16}.

4. EXPERIMENTAL RESULTS AND DATA ANALYSIS

The developed neuro-controller is deployed at the receiver experimental setup in a closed-loop control configuration, as a local observer and corrector³, to accomplish the beam stabilisation process. The performance of the laser communication system on mitigating the beam wandering i.e., reducing the optical signal fluctuation due to effective scintillation^{3,14,15} is continuously measured and intensively investigated. All these results are used to comprehensively analyse and validate the performance improvements attained by incorporating the BWM control system. Some of the experimental results, in communication perspectives: Q-factor, T_a , BER, beam centroid stabilisation, and A_{att} obtained during different weather conditions with and without BWM control are discussed as follows

4.1 General Performance of Atmospheric Turbulent Channel on Modulated Optical Wave

The Q-factor measurement has mostly been extensively used in order to estimate the quality of the optical communication system especially in fiber optics communication^{3,6,8,10}. Therefore, the Q-factor i.e., Q_{att} variations as a function of T_a are investigated using the received data statistics and the Eqns. (4) and (5) during different seasons: very-weak to very-strong C_n^2 conditions without mitigating the beam wandering to understand the general effects of atmospheric channel on the propagating optical wave. All these values are recorded and compared with the measured Q-factor (using BER tester) values and the results are shown in Fig. 6 which exhibits a good agreement between the estimation and the measurement. Further, the results proved that the Q-factor decreases linearly with increase in the A_{att} (decrease in the T_a) due to the atmospheric absorption, scattering and beam wandering effects^{3,14,15}. Since, the beam wandering is unmitigated, the T_a fluctuates arbitrarily and hence the Q-factor varies steeply with the mean value of 2.93.

The transmitter average input power of 10mW is maintained constant and the corresponding Q_{max} is ≈ 6 at the T_{amax} of 90 per cent. The BER performance against the T_a for NRZ-OOK scheme calculated using Eqn. (6) is shown in Fig. 7, therein, the y-axis is truncated to 9.36×10^{-9} . The estimated BER values keep a good agreement with the measured (using

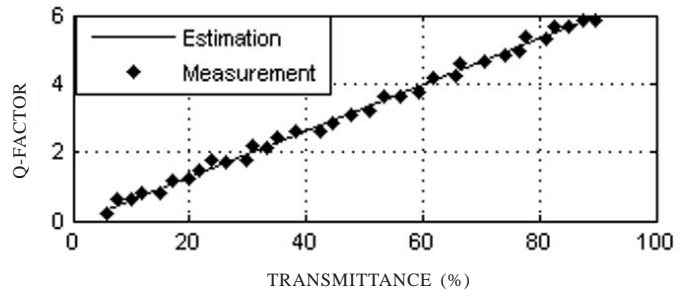


Figure 6. Post-processed Q-factor versus transmittance for OOK-NRZ scheme.

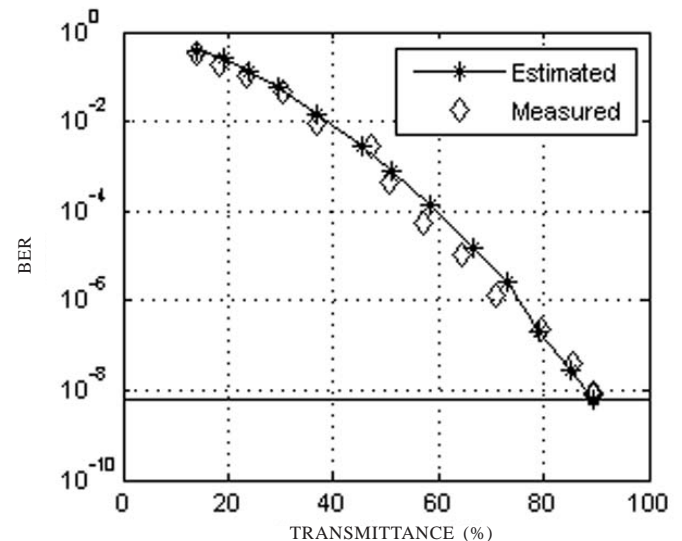


Figure 7. BER against a range of transmittance.

Table 1. BER summary of laser communication data transmission experiments and comments

Season	Date / (Session)	Minimum BER	Maximum BER	Mean BER	Comments on BER trend
Winter	17-12-'14/ (1)	1.80×10^{-7}	4.19×10^{-7}	2.06×10^{-7}	Stable, slightly decreasing
	17-12-'14/ (2)	9.64×10^{-7}	3.72×10^{-6}	8.06×10^{-7}	Variable $\uparrow\downarrow$
	17-12-'14/ (3)	1.67×10^{-7}	4.38×10^{-5}	2.18×10^{-6}	Variable monotonically decreasing
Pre-summer	21-03-'15/ (1)	5.74×10^{-7}	4.93×10^{-4}	8.43×10^{-5}	Variable, conspicuous bump
	21-03-'15/ (2)	1.51×10^{-6}	1.54×10^{-6}	0.38×10^{-6}	Stable with a final increase
	21-03-'15/ (3)	4.35×10^{-5}	4.13×10^{-3}	2.16×10^{-4}	Stable with a final exponential increase
Summer	19-05-'15/ (1)	3.64×10^{-5}	3.63×10^{-5}	3.61×10^{-5}	Only two measurements
	19-05-'15/ (2)	6.45×10^{-9}	6.45×10^{-9}	6.40×10^{-9}	Perfect link: BER \approx 0
	19-05-'15/ (3)	5.78×10^{-5}	4.81×10^{-8}	6.21×10^{-6}	Variable $\uparrow\downarrow$
Monsoon	17-06-'15/ (1)	7.24×10^{-7}	2.72×10^{-6}	7.06×10^{-7}	Variable $\uparrow\downarrow$
	17-06-'15/ (2)	6.78×10^{-5}	4.91×10^{-8}	5.21×10^{-6}	Variable $\uparrow\downarrow$
	17-06-'15/ (3)	1.11×10^{-6}	1.43×10^{-6}	0.42×10^{-6}	Stable with a final increase
Rainy	09-11-'15/ (1)	4.14×10^{-7}	5.33×10^{-4}	7.93×10^{-5}	Variable, conspicuous bump
	09-11-'15/ (2)	2.94×10^{-5}	2.91×10^{-5}	2.93×10^{-5}	Only two measurements
	09-11-'15/ (3)	8.64×10^{-7}	4.72×10^{-6}	7.06×10^{-7}	Variable $\uparrow\downarrow$

BER tester) BER values. Since, the beam wandering is unmitigated, the beam centroid starts fluctuating, so that the T_a decreases. It is observed that the link availability at a BER value of 10^{-6} is related to the Q-factor of ≈ 4.82 following Eqn. (7). The required value of Q-factor to maintain the maximum availability i.e., 99.999 per cent cannot be achieved under all the weather conditions without beam stabilisation system even for increased input power^{6,8,14,15}. The diurnal period cycle of the day during different local seasons: winter, pre-summer, summer, monsoon and rainy, is classified as three sessions: Forenoon (06.00 Hrs to 12.00 Hrs)-(1), Afternoon (12.00 Hrs to 18.00 Hrs)-(2) and Night (18.00 Hrs to 06.00 Hrs)-(3). The BER is continuously measured in all the sessions without BWM control and the results are recorded in the BER data logging files in MATLAB environment. The minimum, maximum and mean values of the BER measured on a day in each season for three sessions are given in Table 1. These measurements are carried out at the ATM data rate. The measurement data clearly evidences that the BER continuously fluctuates and this trend degrades/decreases the overall performance: Reliability and quality, of the FSOC system. The similar trends are observed on most of the days in each local season due to the atmospheric effects and other disturbance agents as discussed in Section-I. This happens purely because of the received power fluctuation at the detector plane due to scintillation and beam wandering effects. Therefore, mitigating the beam wandering effects to change this trend to improve the overall performance of the laser communication system becomes significant.

4.2 Analysis of Beam Centroid Stabilisation and Atmospheric Attenuation

As the C_n^2 increases, the propagating optical beam will experience larger degradation, centroid wandering and break-up from the transmission axis which will disconnect the data reception. The profile of the received beam centroid wander is recorded using the science camera in IR mode at the output

(eye-piece) of the telescope to understand the beam wandering displacements. The range of the C_n^2 observed on 17th June 2015 using the developed model, as in Eqn. (3), is varied from weak to strong. The Gaussian beam of diameter 4mm profile recorded on the same day with the BWM on and off conditions are shown in Fig. 8 (a) and 8 (b), respectively. The beam retains its characteristics, shape and is well centered once the BWM control is turned on; otherwise the beam experiences the degradation and loses its position stability as shown in Fig. 8(b). The centroid coordinates are off center up to the magnitude of 0.2 mm and 1.2 mm in the x and y directions respectively during this particular observation. In the strong C_n^2 conditions, once the beam wandering is unmitigated, then the beam experiences a larger deviation and starts breaking-up the data link. Geometrical interpretation of the wavefront (global) of the received optical beam at the communication detector plane is modeled using the beam centroid position information: x, y displacements/positions and radial distance (γ), obtained from the OPD using the geometrical theory²⁶. Some of the time series geometrical interpretations of beam wavefront (global) tilts estimated on 05th July 2015 are shown

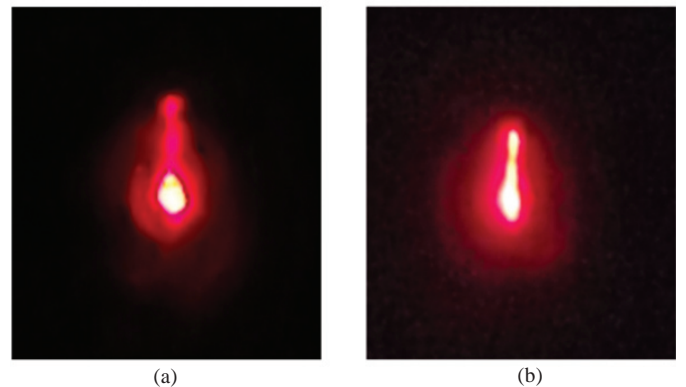


Figure 8. Beam spot when beam wandering (a) mitigated and (b) unmitigated. Note that the axes are compressed of mm scales.

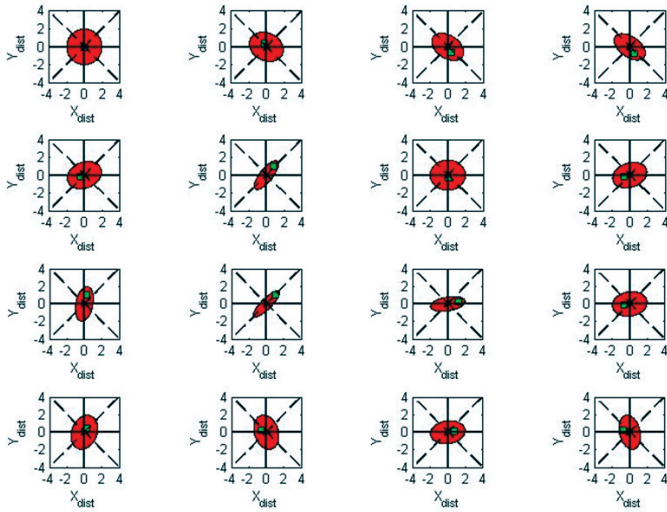


Figure 9. Geometrical interpretation of beam wavefront (global) profile appears on the detector plane. Note that the beam spot and radial distance are illustrated by red and green colors, respectively.

in Fig. 9 and therein, the (1,1) illustrates the beam wandering mitigated wavefront profile while the others are corresponding to the unmitigated and they clearly exhibit that the beam centroid randomly wanders on the detector plane. These results evidence that the BWM control becomes significant to couple the power in bucket (PiB) i.e., telescope collected power, to the communication detector for the successful installation of a reliable laser communication system. A transmissiometer working with 550 nm optical beam is used to measure the visibility conditions of the atmospheric channel during the experimentation as used in⁸. The atmospheric attenuation is continuously estimated using the measured values of transmitted and received power during different visibility conditions with and without mitigating the beam wandering effects and the results are shown in Fig. 10. The main observations when the beam wandering is not mitigated are (i) attenuation varies from 3.12 dB/km to 127 dB/km, (ii) attenuation increases rapidly when the visibility approaches to the lowest value, (iii) different values of attenuation are measured for a value of visibility as shown in Fig. 10 by the error-bars and (iv) variations in the attenuation for a value of visibility is not linear with the value

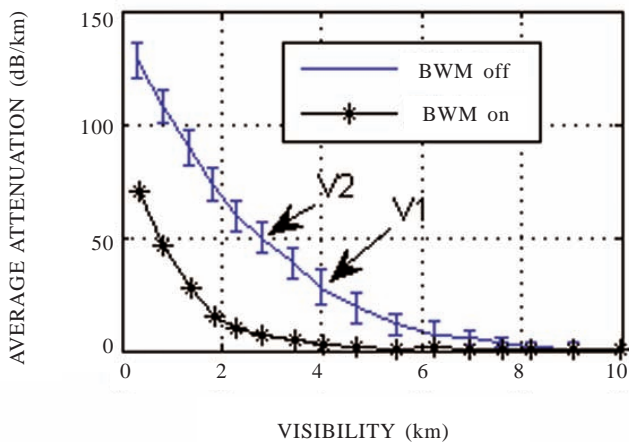


Figure 10. Average visibility versus average attenuation.

of visibility, for example, the variation for the visibility values of 3 km and 4 km are 15 dB/km (marked by V1) and 20 dB/km (marked by V2) respectively. Further, the observations (iii) and (iv) clearly evidence that atmospheric fluctuations could result in beam wandering^{3,8,14,15}. The observations are significantly improved once the beam wandering is mitigated as (i) attenuation varies from 3.12 dB/km to 67.23 dB/km, (ii) the pattern/rate of change of attenuation for the changes of visibility are significantly controlled and (iii) almost constant attenuation is observed for a value of visibility. These results clearly exhibit the improvement attained in coupling the PiB to communication detector by mitigating the beam wandering effects. Further, beam wandering mitigation is not required when the visibility appears above the 8 km.

4.3 Quality Metrics and Reliability of Laser Communication System

The impact of atmospheric channel fluctuation on the receiver decision threshold value is estimated based on the signal statistics obtained from the eye-diagram. The results corresponding to the signal obtained from the TIA when the BWM control off and on conditions are shown in the upper plots of Fig. 11. This plot i.e., distribution pattern (histogram) is designed using 50000 ensembles (each). There, the decision threshold is 0V. In the absence of BWM control, the received signal distribution becomes heavily distorted and is no longer distinguishable during moderate C_n^2 conditions which results in the decreased Q-factor and increased BER values, whereas in the presence of the BWM control even during the strong C_n^2 condition, the received signal distribution for bits ‘1’ and ‘0’ are equally spaced and comparable for both sides of the decision threshold level and the bits ‘1’ and ‘0’ are clearly distinguishable. The maximum count value of ≈ 10000 for bit ‘0’ at -0.2 V and the count value of 15000 for bit ‘1’ at 0.2 V with many voltage level distributions in between these two levels are observed when BWM control is off, whereas in on, the maximum count value of ≈ 48000 for bit ‘0’ at -0.18 V and ≈ 58600 for bit ‘1’ at 0.18V with the ≈ 0 V distribution in between these two levels are observed during the strong C_n^2 condition. The distributions of measured Q-factor values corresponding to the upper plots of Fig. 11 are as shown in the lower plots of Fig. 11 which clearly exhibits that the Q-factor distribution is highly random once the beam wandering is not mitigated, whereas if mitigated, the Q-factor value of 6.4 appears for the count value of 859 during the strong C_n^2 . The BER is measured during different C_n^2 conditions for the beam wandering control under both off and on conditions and the $\log_{10}(BER)$ histogram results are as shown in Fig. 12. Note that the BER value is truncated to 10^{-8} to represent the lowest (1 bit error) BER i.e., 6.451×10^{-9} ($\log_{10}(BER) = -8.19$) at the ATM data rate instead of zero BER. The main observations of the $\log_{10}(BER)$ when the beam wandering control is off are (i) values vary from -8.19 to 0, (ii) maximum count value is observed at the -2.78, (iii) distribution of values are highly random during the different local seasons and do not fit with any standard distributions and (iv) more than 90 per cent of error is obtained during some measurement, whereas, in the on condition (i) values vary from -8.19 to -7.1 i.e., BER of 6.45

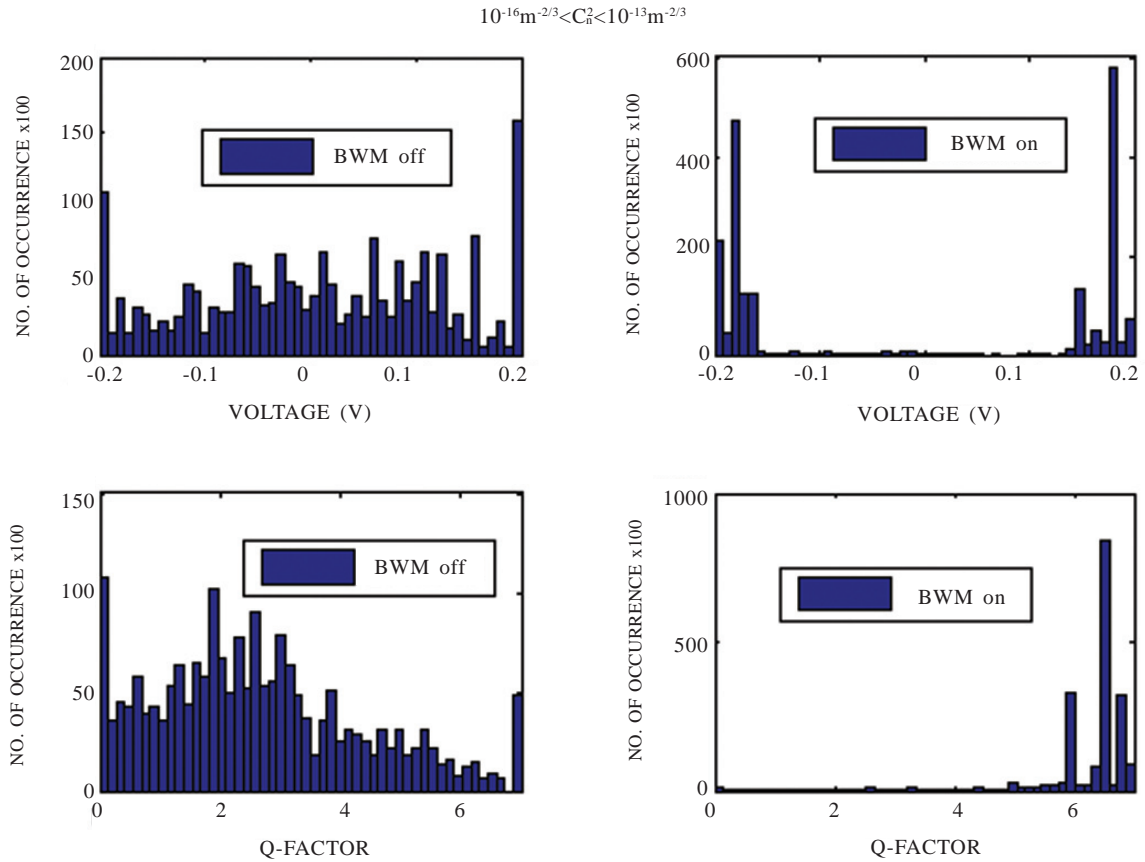


Figure 11. Distribution of received data ‘0’ and ‘1’ (upper) and the corresponding Q-factor (lower).

$\times 10^{-9}$ to 7.74×10^{-8} , (ii) maximum count value is observed around the -7.71 i.e., BER of 1.93×10^{-8} , (iii) the distribution approximately fits with the Gamma distribution and (iv) less than 1.48×10^{-4} per cent errors are observed during the daylong experimentation conducted in different atmospheric conditions. These results exhibit the improvements attained in the quality metrics and reliabilities of the developed laser communication system by mitigating the beam wandering effects. However, the BER reaches the maximum value of around 8.71×10^{-4} i.e., 135090 error bits during the very strong C_n^2 condition even in the presence of beam wandering mitigation control. This is due to the wavefront aberrations and it has to be resolved by incorporating the adaptive optics to improve the reliability of the laser communication system further which is set for the near future research work.

5. CONCLUSION

Significance of beam wandering mitigation is explained. Quantitative evaluation of atmospheric turbulence channel effects on propagating optical wave is detailed. Construction of the laser communication Tx and Rx experimental setup and functionality of the neuro-controller are described. The variations of the Q-factor and BER in terms of T_a are experimentally studied. The statistics related to the diurnal period profile of the measured BER are listed and discussed. The optical wavefront geometry during different C_n^2 conditions is interpreted. The improvements attained on the Average A_{att} , received voltage and Q-factor are analysed with and without mitigating the beam wandering effects. The improved beam stability at the communication detector and coupling of PiB to the detector are highlighted.

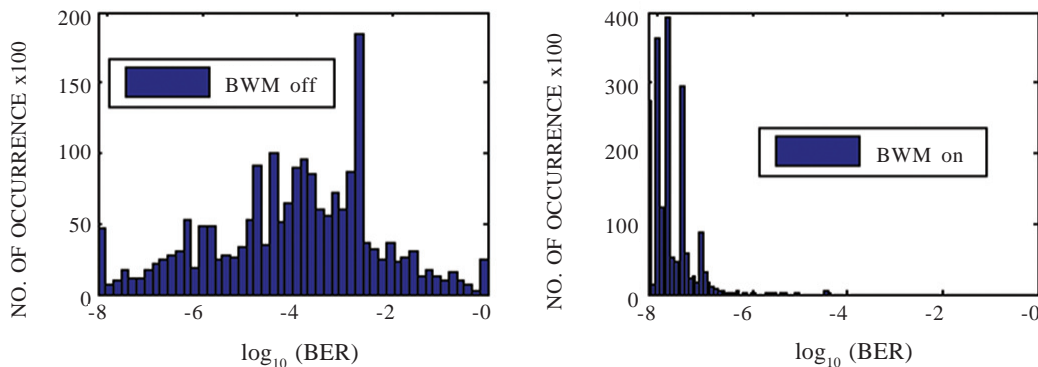


Figure 12. Bin frequency of measured BER.

REFERENCES

1. Leitgeb, E. Free space optics in different (civil and military) application scenarios in combination with other wireless technologies. *In* 16th International Telecommunications Network Strategy and Planning Symposium (Networks), 2014, pp.1-7.
doi: 10.1109/NETWKS.2014.6959207
2. Yoshinori, Arimoto. Developing a new free-space optical communication terminal that realizes high-speed broadband communications. NICT News, No. 392, 2010, pp. 1-5.
3. Raj, A.A. Intensity feedback based beam wandering mitigation in free space optical communication using neural control technique. *EURASIP J. Wireless Commun. Networking*, 2014, 1–18.
doi: 10.1186/1687-1499-2014-160.
4. Bazil Raj, A. Low cost beam steering system for FSOC to SMF coupling. IEEE International Conference, Advances in Engineering, Science and Management, Nagapattinam, 2012, pp.49–54.
5. Gappmair, W. Further results on the capacity of free-space optical channels in turbulent atmosphere. *IET Commun.*, 2011, **5**(9), 1262-1267.
doi: 10.1049/iet-com.2010.0172
6. Barrios, Ricardo & Dios, Federico. Wireless optical communications through the turbulent atmosphere: A review. Edited by Narottam Das, Optical Communications Systems, 2012, pp. 3-40, InTech, Croatia.
7. Matsumoto, M. An alternative access technology for next generation networks based on full-optical wireless communication links. *In* the Innovations in NGN: Future Network and Services, K-INGN, First ITU-T Kaleidoscope Academic Conference, Geneva, 2008, pp.221-228.
doi: 10.1109/kingn.2008.4542269
8. Arockia, Bazil Raj, A. Free space optical communication: System design, modeling, characterization and dealing with turbulence. 2015, De Gruyter.
9. Arockia, Bazil Raj, A. A direct and neural controller performance study with beam wandering mitigation control in free space optical link. *Opt. Memory Neural Network (Info. Opt.)*, 2014, **23**(3), 111-129.
10. Mahdiah, M.H. & Pournoury, M. Atmospheric turbulence and numerical evaluation of bit error rate (BER) in free-space communication. *Opt. Laser Technol.*, 2010, **42**(1), 55-60.
doi: 10.1016/j.optlastec.2009.04.017
11. Kostas, P. Peppas. Capacity analysis of dual amplify-and-forward relayed free-space optical communication systems over turbulence channels with pointing errors. *J. Opt. Networking Commun. Networking*, 2013, **5**(9), 1032-1042.
12. Ansari, Imran shafique. Impact of pointing errors on the performance of mixed RF/FSO dual-hop transmission systems. *IEEE Wireless Commun. Lett.*, 2013, **2**(3), 351-354.
13. Feng, Feng. Aberration correction for free space optical communications using rectangular Zernike modal wavefront sensing. *J. Lightwave Technol.*, 2014, **32**(6), 1239-1245.
doi: 10.1109/JLT.2014.2301634
14. Andrews, L.C. Beam wandering effects on the scintillation index of a focused beam. *In* Proceedings SPIE 5793, Atmospheric Propagation II, pp.1-10, 2005.
15. Mohan, Swati. Pointing, acquisition, and tracking architecture tools for deep-space optical communications. Proceedings SPIE 8971, 2014.
16. Arockia, Bazil Raj, A. Mitigation of beam fluctuation due to atmospheric turbulence and prediction of control quality using intelligent decision-making tools. *Appl. Opt.*, 2014, **53**(15), 3796-3806.
doi: 10.1364/AO.53.003796
17. Raj, A.A. & Padmavathi, S. Statistical analysis of accurate prediction of local atmospheric optical attenuation with a new model according to weather together with beam wandering compensation system: a season-wise experimental investigation. *J. Modern Opt.*, 2016, pp.1-16.
doi: 10.1080/09500340.2016.1140840
18. Arockia, Bazil Raj, A. Real-time measurement of meteorological parameters for estimating low-altitude atmospheric turbulence strength (C_n^2). *IET Sci. Meas. Technol.*, 2014, **8**(6), 459-469.
19. Perez, Joaquin. Experimental characterization and mitigation of turbulence induced signal fades within an ad-hoc FSO networks. *Opti. Express*, 2013, **22**(3), 3208-3218.
20. Bendersky, Sergey. Atmospheric optical turbulence over land in middle east coastal environments: Prediction modeling and measurements. *Appl. Opti.*, 2004, **43**(20), 4070-4079.
doi: 10.1364/AO.43.004070
21. Arockia, Bazil Raj, A. & Selvi, J. Arputha Vijaya. Comparison of different models for ground-level atmospheric turbulence strength (C_n^2) prediction with a new model according to local weather data for FSO applications. *Appl. Opt.*, 2015, **54**(4), 802-815.
doi: 10.1364/AO.54.000802
22. Dror, Itai. Accurate method for prediction of atmospheric transmission according to weather. *Opti. Eng.*, 1996, **35**(9), 2548-2555.
doi: 10.1117/1.600863
23. Arockia, Bazil Raj, A. & Selvi, J. Arputha Vijaya. Comparison of different models for ground-level atmospheric attenuation prediction with new models according to local weather data for FSO applications. *J. Opt. Commun.*, 2015, **36**(2), 181–196.
doi: 10.1515/joc-2014-0054
24. Muthiah, D. & Arockia, Bazil Raj A. Implementation of high-speed LFSR design with parallel architectures. *In* the IEEE International Conference on Computing, Communication and Applications, Dindugal, 2012, pp.1–6.
doi: 10.1109/iccca.2012.6179137
25. Arockia, Bazil Raj, A. Design of cognitive decision making controller for autonomous online adaptive beam steering in free space optical communication system.

Wireless Pers. Commun., 2015, **84**, pp.765–799.

26. Zheng, Chongwei. Propagation of elliptical Gaussian beam passing through apertured paraxial optical systems. *Optik–Int. J. Light Electron. Opt.*, 2014, **125**(1), pp.264. doi: 10.1016/j.ijleo.2013.06.053

ACKNOWLEDGMENT

The authors would like to sincerely thank the Extramural Research & Intellectual Property Rights (ER&IPR), Defense Research and Development Organisation (DRDO), New Delhi, India, for the financial support for lab establishment, experimentation and constructive comments and suggestions for the successful completion of this and subsequent works.

CONTRIBUTORS

Dr A. Arockia Basil Raj, received his BE (Electronics and Communication Engineering) from the Bharathidasan University, Tiruchirappalli, India, his ME (Communication Systems) and PhD (Information and Communication Technology) from the Anna University, Chennai, India. Presently, he is an Assistant Professor in Defence Institute of Advanced Technology, Pune, Maharashtra, India. His current research interests cover the digital modulation, free-space and adaptive optics, hardware design

of neural network, feedback control, VLSI, signal processing, microrobotics, mechatronics, T&M instrument design, radar signal processing and empirical modelling.

He has contributed significantly in developing the experimental setups, designing the neuro-controller and building the digital architecture inside the FPGA to realize the hardware assisted control action in a closed-loop control configuration to stabilize the beam that arrive the FSM.

Dr S. Padmavathi, received her BE (Electrical and Electronics Engineering) from Madurai Kamarajar University, Madurai, Tamil Nadu, India and ME (Computer Science and Engineering) and PhD (Information and Communication Engineering) from Anna University, Chennai, India. Currently, she is working as an Associate professor in the Department of Computer Science and Engineering, Thiagarajar College of Engineering, Madurai, Tamil Nadu, India. Her current research interests cover the Free-space and adaptive optics, scheduling algorithms, cloud computing and parallel computing.

She has contributed significantly in validating the prediction accuracy of atmospheric attenuation and turbulence strength in terms of local weather data. She also performed the experiment over a longer period and statistically analyzed the data in terms of different communication quality metric parameters.